Supplementary Material

Interfacial defect reduction enhances universal power law response in Mo-SiN_x granular metals

Michael P. McGarry[1], Simeon J. Gilbert[1], Luke Yates, Melissa L. Meyerson[1], Paul G. Kotula[1], William B. Bachman[1], Peter A. Sharma[1], Jack D. Flicker[1], Michael P. Siegal[1], and Laura B. Biedermann[1]*

[1]Sandia National Laboratories, Albuquerque, NM 87185, USA

[*]Corresponding author e-mail: lbieder@sandia.gov

FIG. S9. Nyquist plots of the GM samples which corresponds to the frequency data in Figure 6. The dense array of solid cyan circles are measured data, the solid lines are the ZView fit a) φ = 0.25 b) φ = 0.30 c) φ = 0.35 10

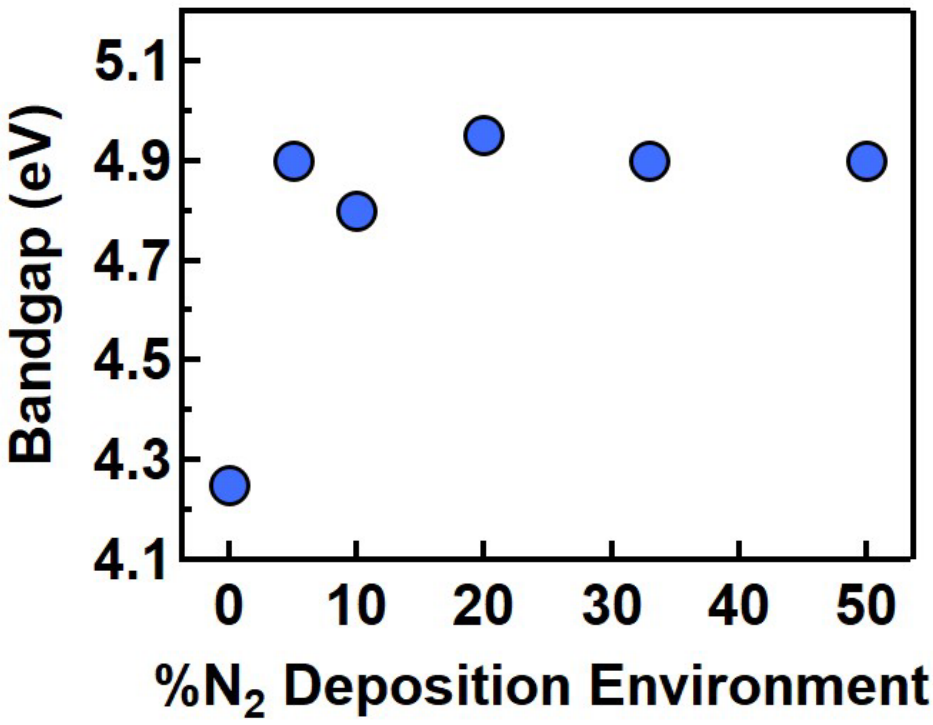

FIG. S1. The SiN_x bandgap as determined from Tauc plots of the optical transmission spectrum. Optical transmission was measured using a PerkinElmer Lambda 900 UV/Vis/NIR spectrophotometer.

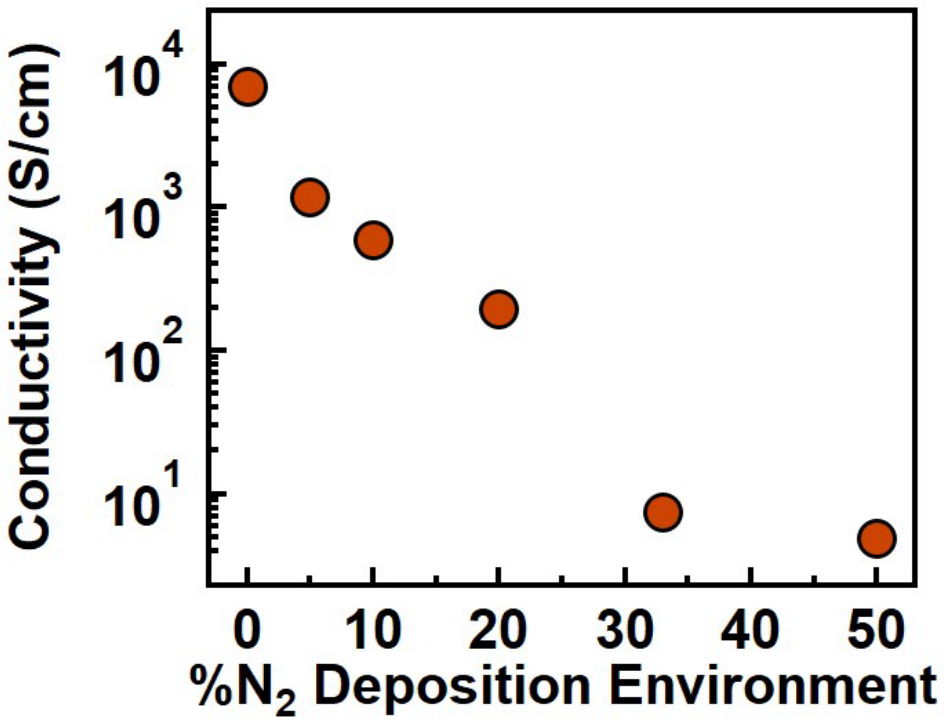

FIG. S2. The conductivity of Mo films deposited with a power of 60 W in varying Ar/N_2 environments.

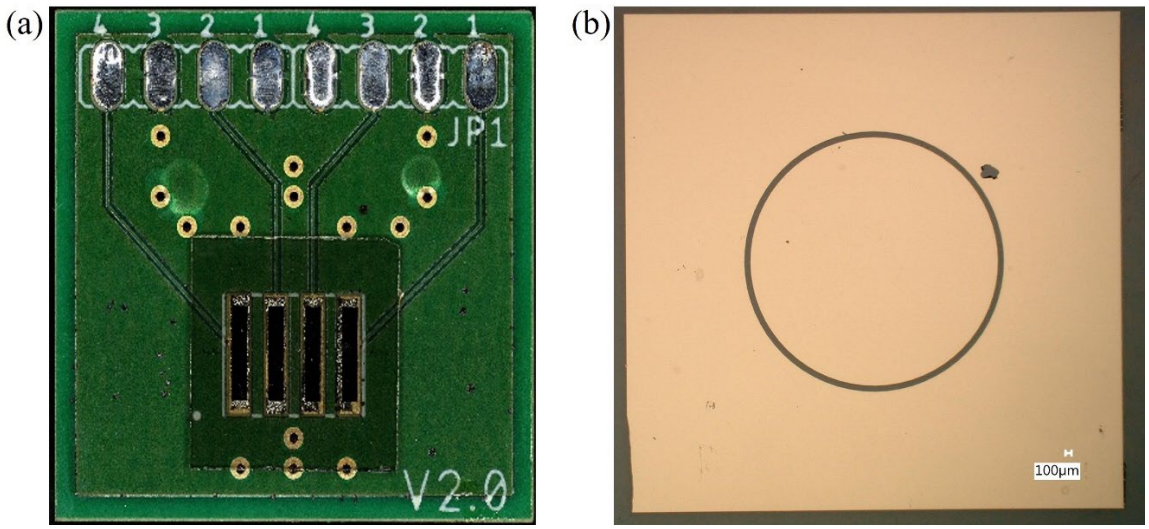

FIG. S3. (a) Optical micrograph of GM sample mounted on a custom PCB with parallel bar electrodes. (b) Optical micrograph of CTLM electrode geometry with 0.1 mm electrode gap. The circular ring defines the active area.

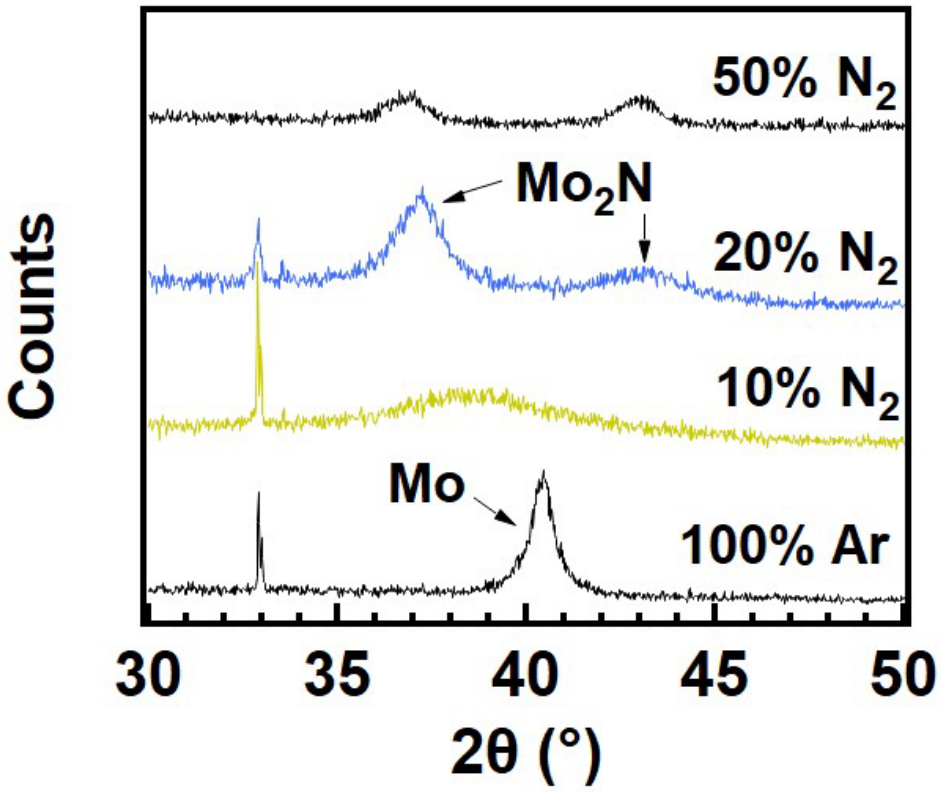

FIG. S4. XRD spectra of Mo films deposited with powers of 60 W in varying Ar/N_2 environments.

X-ray diffraction spectra of Mo films are shown in Fig. S4. The sharp peak at 33º is from the sample holder. In 100% Ar, the Mo (110) peak is observed at 40.4º. The introduction of 10% N_2 reduces sample crystallinity with a single broad, weak peak centered at ~38.5º; 10% N_2 was not sufficient to fully convert the Mo into Mo_2N. For the 20% N_2 sample, the Mo_2N (111) and (200) peaks are observed at 37.2º and 43.1º, respectively. In 50% N_2, the Mo_2N peaks are still observed, but with a lower intensity indicating lower crystallinity compared to the 20% N_2 sample. This lower crystallinity may indicate a Mo_2N_x composition where $x > 1$. A Bruker D2 Phaser benchtop XRD system with Cu Kα radiation was used for these measurements.

We compare VRH and Arrhenius conductivity mechanisms by fitting the same conductivity data on different axes, $T^{-1/2}$ and T^{-1}, in Fig. S5. A single slope fits the VRH $T^{-1/2}$ temperature range, as shown in Fig. 3 of the manuscript. For $\varphi = 0.25$ in 100% Ar and for $\varphi = 0.30$ in 10% N_2, a single slope fits the Arrhenius T^{-1} temperature dependency and has a reasonable fitting across the measured temperature range (see Fig. 5a). Conversely, for $\varphi = 0.3$ and 0.35 in 100% Ar, subsets of the thermal dependance can be fit to the Arrhenius T^{-1} temperature dependency; two linear fitting regimes are required to fit the range 20 K to 300 K (see Fig. S5b). Table S1 tabulates the quality of the fits in Fig. S5 as well as the temperature range in which those linear fits were made.

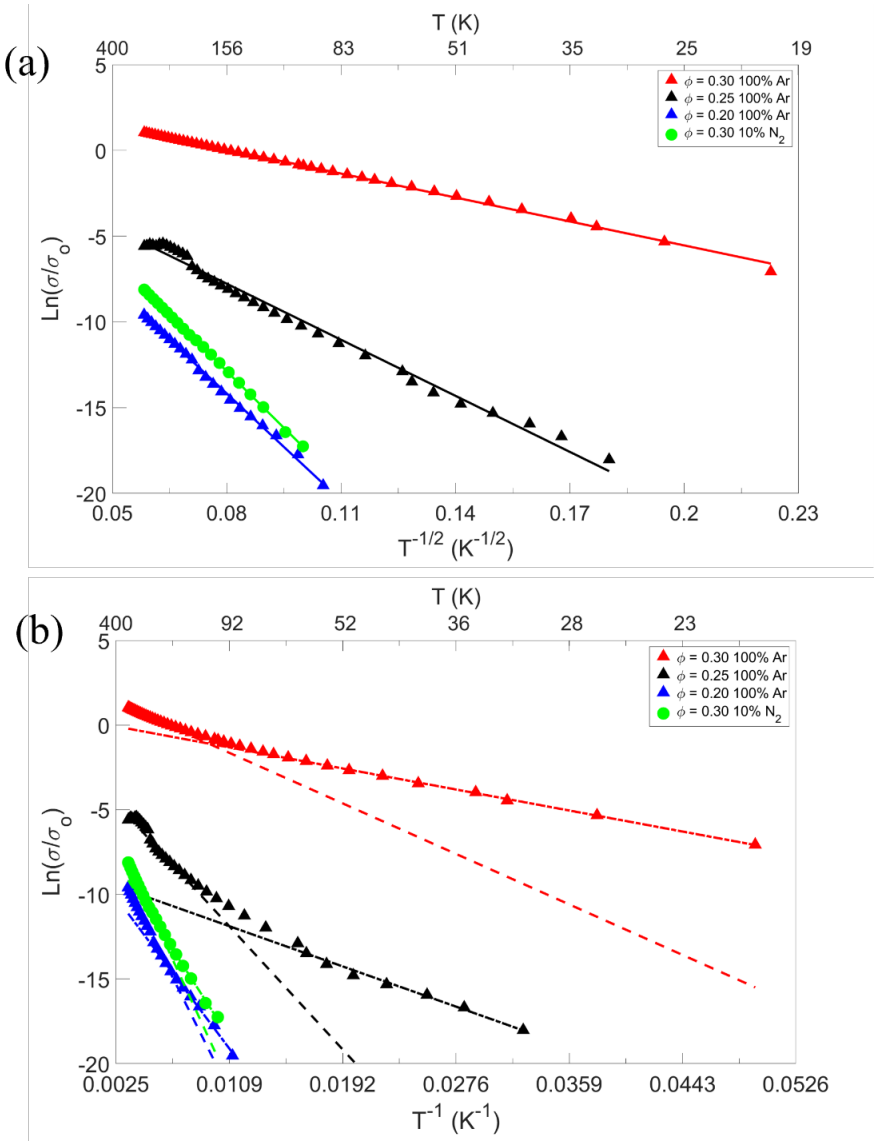

FIG. S5. (a) Conductivity vs. $(T)^{-1/2}$ plot of the data to fit VRH conduction. (b) Conductivity vs. $1/T$ plot of the data to fit Arrhenius conduction.

TABLE S1. Linear fit temperature ranges and goodness of fit parameter, R^2, for the data in Fig. S5 for VRH and Arrhenius conduction.

Sample	VRH		Arrhenius	
	Fit temp. range (K)	R^2	Fit temp. range (K)	R^2
φ = 0.20 100% Ar	90 – 300	0.998	91 – 300	0.987
φ = 0.25 100% Ar	31 – 300	0.990	31 – 100	0.974
			100 – 300	0.985
φ = 0.30 100% Ar	20 – 300	0.998	20 – 125	0.995
			125 – 300	0.995
φ = 0.30 10% N_2	100 – 300	1.00	100 – 300	0.995

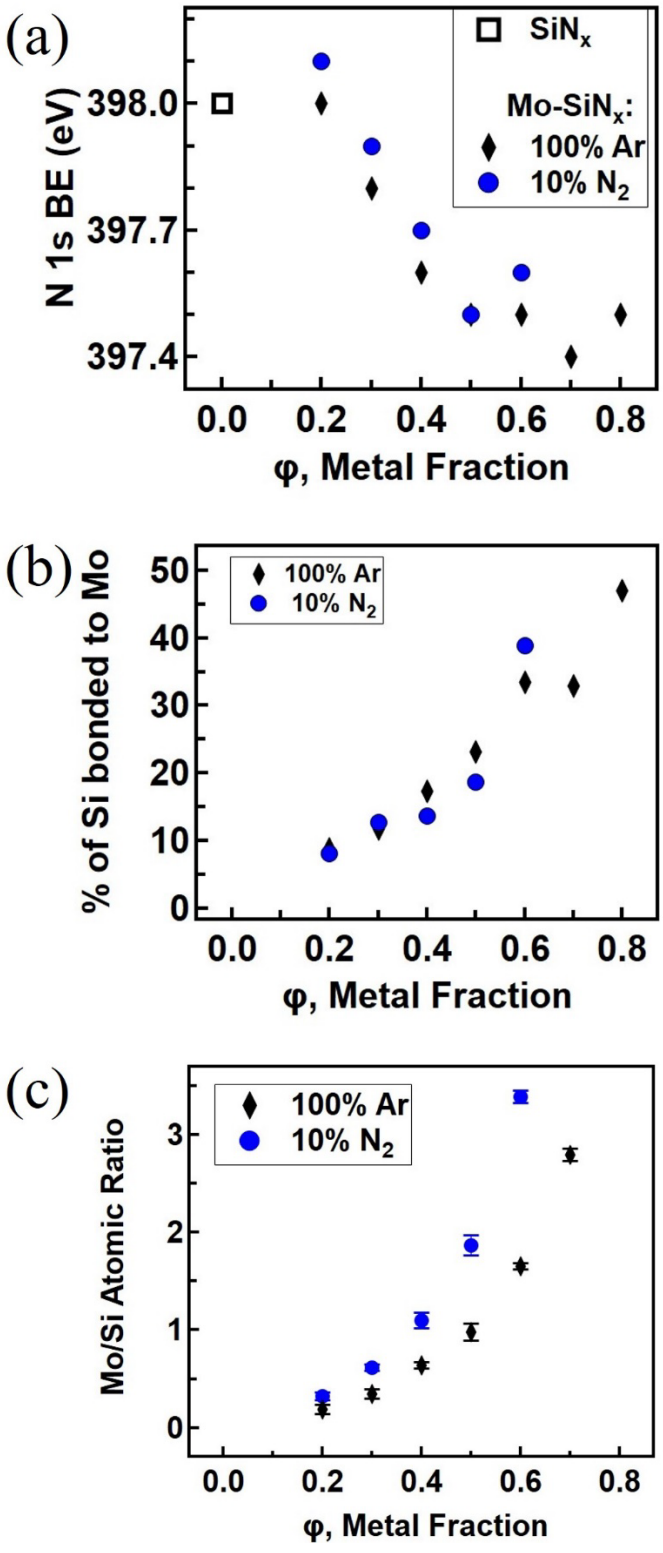

FIG. S6. (a) Comparison of the nitrogen 1s binding energy (BE) from XPS for various Mo-SiN_x samples. (b) The percentage of silicon atoms bound to Mo as determined by the ratio for silicon 2p XPS peaks. (c) The Mo/Si atomic ratios as determined by XPS for various Mo-SiN_x samples.

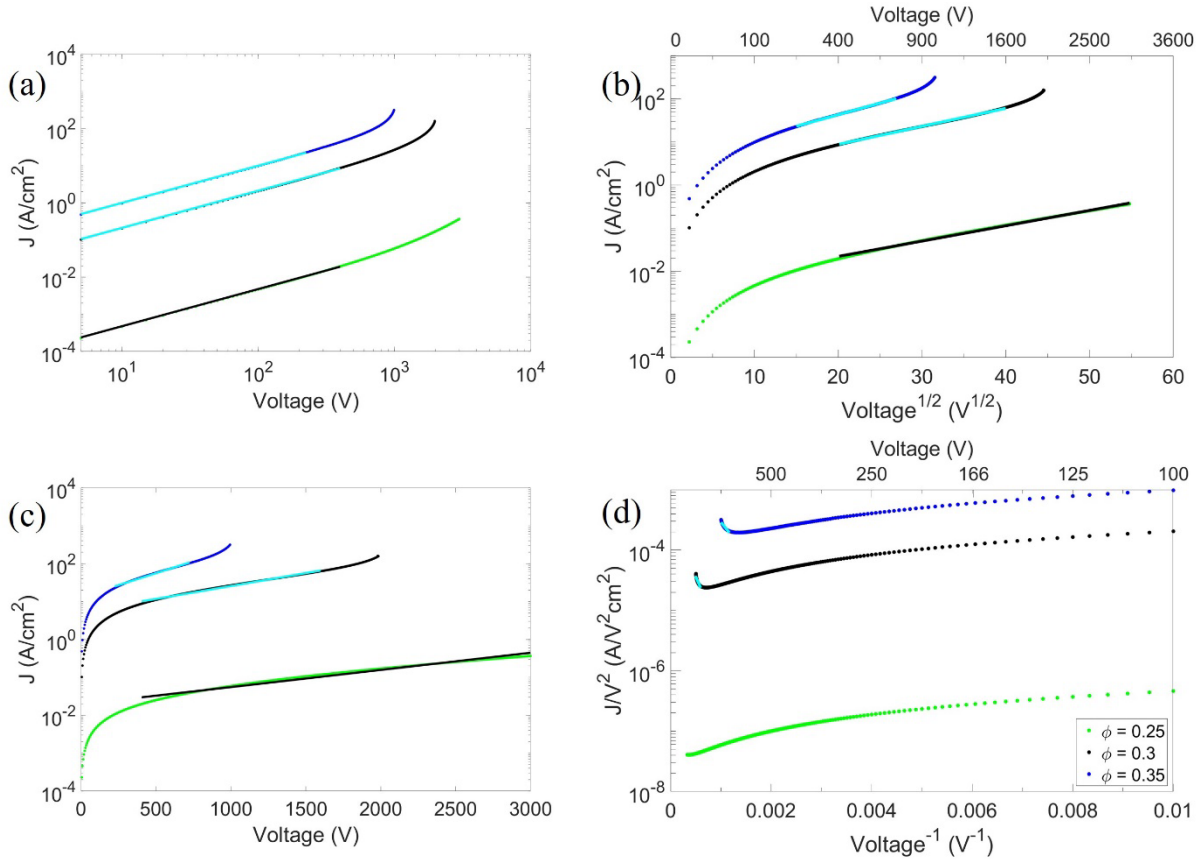

FIG. S7. *J-V* graphs of the same data plotted on selected axes to linearize the transport regimes; the cyan line in the graphs highlight the linearized portions for $\varphi = 0.3$ and 0.35, while the black line in the graphs highlight the linearized portion for $\varphi = 0.25$. The φ legend in (d) applies to all plots. (a) Ohmic regime: J vs. V on a log-log plot (b) Classical Poole-Frenkel model: J vs. $V^{1/2}$ on a log-linear plot (c) 2CPF Poole-Frenkel model: J vs. V on a log-linear plot (d) Fowler-Nordheim regime: J/V^2 vs. $1/V$ on a log-linear plot.

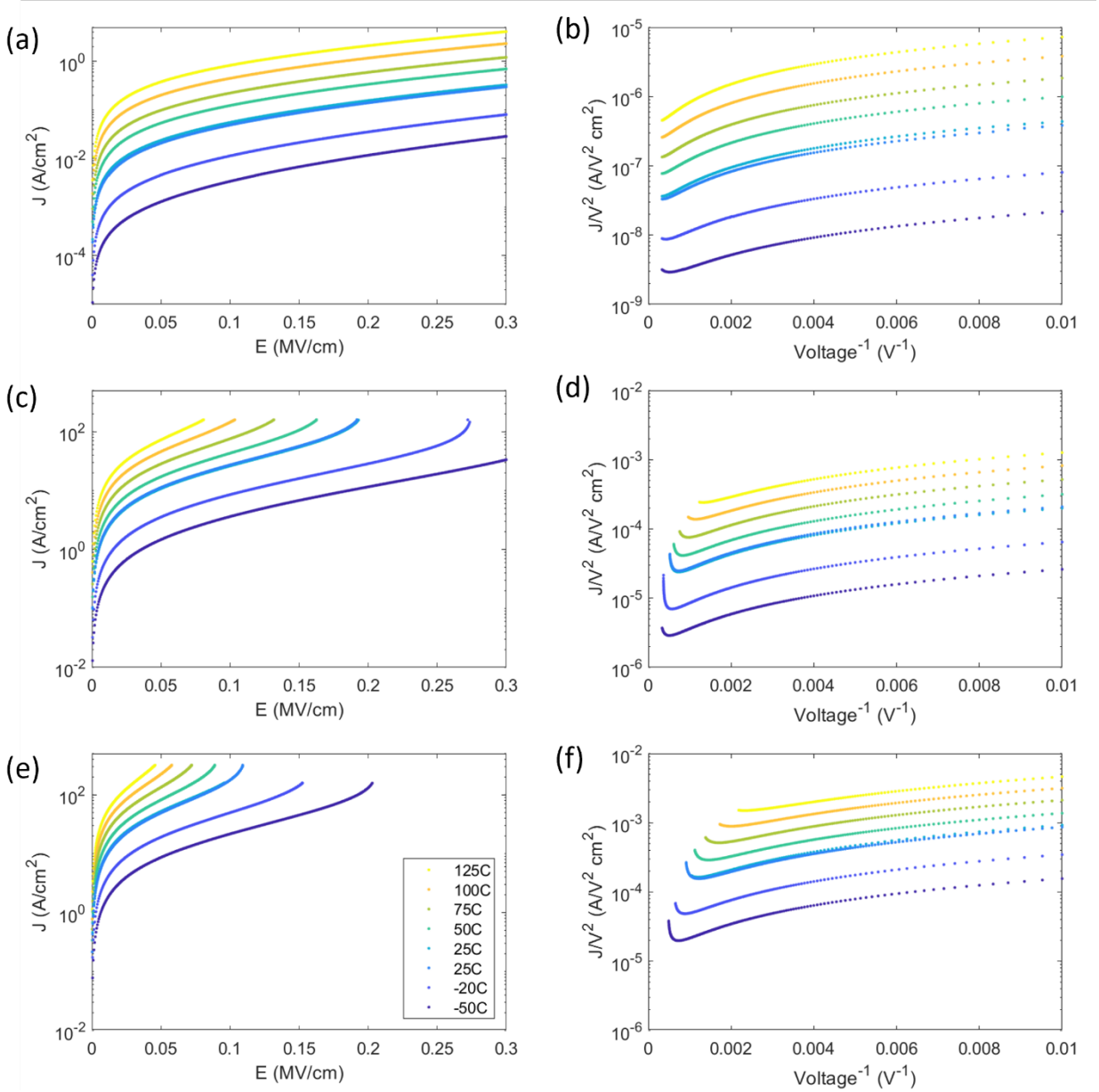

FIG. S8. Temperature-dependent *J-E* characteristics of $\varphi = 0.25$ (a, b), $\varphi = 0.30$ (b, c), and $\varphi = 0.35$ (e, f) GM samples grown in 10% N_2; the temperature legend in (e) applies to all plots. Linearization to highlight Fowler-Nordheim transport (b, d, f) indicates that all three GM samples demonstrate Fowler-Nordheim transport at -50 °C.

Two separate probe stations were used for these measurements, hence the repeated 25 °C sweeps to verify consistency. A Keysight B1505A Source Measurement Unit (SMU) was used for heated *J-E* sweeps and a Keysight B1500A was used for cooled *J-E* sweeps.

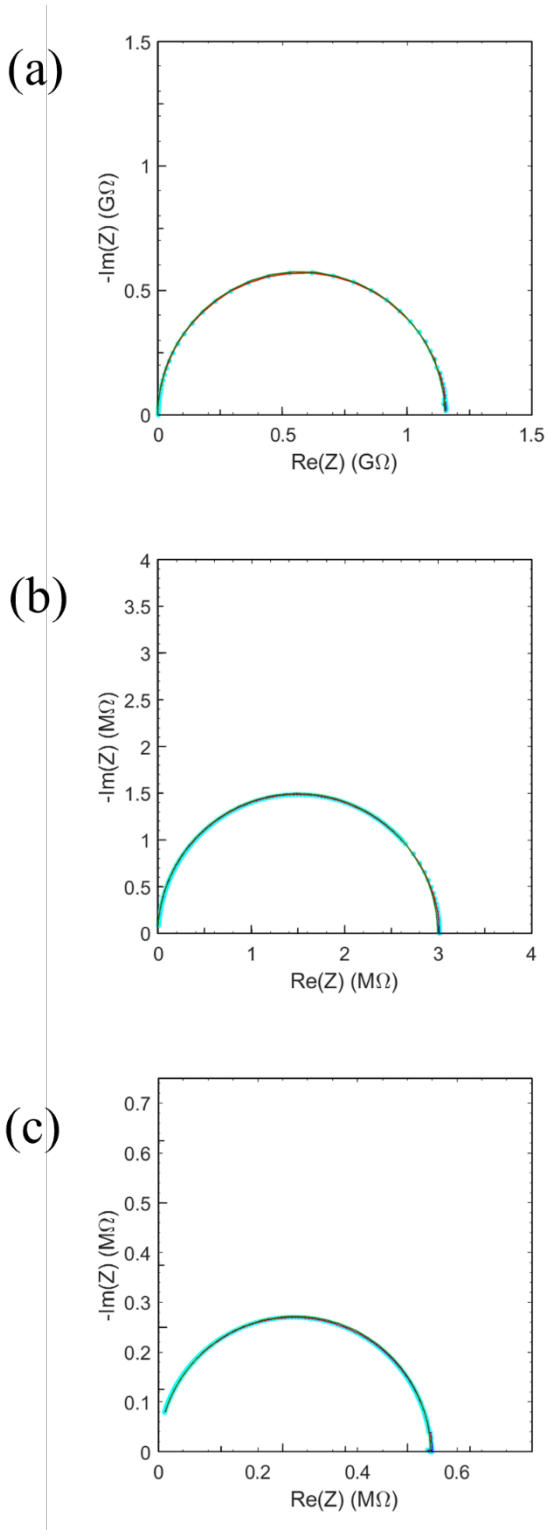

FIG. S9. Nyquist plots of the GM samples which corresponds to the frequency data in Figure 6. The dense arrays of solid cyan circles are measured data, the solid lines are the ZView fit. GM metal fractions are (a) $\varphi = 0.25$, (b) $\varphi = 0.30$, and (c) $\varphi = 0.35$.